K isotopes as a tracer of seafloor hydrothermal alteration

Christopher A. Parendo[a,1], Stein B. Jacobsen[a], and Kun Wang[a,2,3]

[a]Department of Earth and Planetary Sciences, Harvard University, Cambridge, MA 02138

Edited by David Walker, Columbia University, Palisades, NY, and approved January 6, 2017 (received for review June 7, 2016)

At ocean spreading ridges, circulation of seawater through rock at elevated temperatures alters the chemical and isotopic composition of oceanic crust. Samples obtained from drilling into ocean floor and from ophiolites have demonstrated that certain isotope systems, such as $^{18}O/^{16}O$ and $^{87}Sr/^{86}Sr$, are systematically modified in hydrothermally altered oceanic crust. Although K is known to be mobile during hydrothermal alteration, there have not yet been any K-isotope analyses of altered oceanic crustal materials. Moreover, the $^{41}K/^{39}K$ of seawater was recently found to be significantly higher than that of igneous rocks, so the addition of seawater K to oceanic crust would be expected to generate $^{41}K/^{39}K$ variations in affected rocks. Here, we report high-precision $^{41}K/^{39}K$ measurements for samples from the Bay of Islands ophiolite, and we document large variations in $^{41}K/^{39}K$, covarying with previous determinations of $^{87}Sr/^{86}Sr$. Our data indicate that analytically resolvable $^{41}K/^{39}K$ effects arise in oceanic crust as a result of hydrothermal alteration. This finding raises the possibility that $^{41}K/^{39}K$ can be used as an effective tracer of oceanic crust recycled into the mantle, as a diagnostic criterion by which to identify ancient fragments of oceanic crust, and as a constraint on the flux of K between oceanic crust and seawater.

potassium isotopes | hydrothermal alteration | ocean crust | ophiolite

Hydrothermal circulation occurring at the seafloor exerts a profound influence over the distribution of elements among the earth's oceans, crust, and mantle. According to geophysical and geochemical estimates, the volume of the oceans is circulated through ridge axes on a timescale of tens of millions of years, and through ridge flanks on a timescale of tens to hundreds of thousands of years (1, 2). Heat transfer associated with hydrothermal circulation is a critical factor controlling processes of magma crystallization at midocean ridges (3) and, hence, the differentiation of oceanic crust and depleted mantle. Additionally, interaction of seawater and rock over a range of temperatures entails diverse chemical reactions, and results in significant elemental fluxes between seawater and oceanic crust.

One approach to quantifying these fluxes is to measure chemical and isotopic variations imparted to oceanic crust by hydrothermal alteration (4, 5). Such measurements of hydrothermally altered crust have been useful in constraining estimates for the hydrothermal fluxes of particular elements into or out of seawater (6–8). Characterizing the elemental and isotopic composition of altered crust also provides a means of tracking oceanic crust as it is subducted, mixed into the mantle, and incorporated into island–arc, ocean–island, and midocean-ridge volcanic products (9–11). For these purposes, $^{18}O/^{16}O$ and $^{87}Sr/^{86}Sr$ ratios have been used extensively, and a number of other isotope systems have been used as well.

Potassium is known to be mobile during seafloor hydrothermal alteration. Studies of hydrothermal vent fluids near ridge axes have documented that, in high-temperature environments, K is leached from oceanic crust (12, 13). However, studies of in situ oceanic crust sampled by drilling reveal that altered basalts have much higher K content than fresh midocean-ridge basalt (MORB), indicating a net flux of K into the rock (6–8, 14, 15). Measured pore-water profiles also indicate consumption of K by oceanic crust at lower temperatures (16). These observations are consistent with experimental work showing that K is leached from basalt at temperatures greater than 150 °C, but consumed by basalt at temperatures less than 70 °C (17). Until recently it was not feasible to test how these alteration processes affected the $^{41}K/^{39}K$ ratios of oceanic crust, owing to limitations in the precision of the measurement. New analytical methods have, however, made high-precision determination of $^{41}K/^{39}K$ ratios possible (18, 19).

For this study, we have analyzed six samples from the Blow Me Down (BMD) massif of the Bay of Islands (BOI) ophiolite, Newfoundland, Canada, for $^{41}K/^{39}K$ ratios, to test whether seafloor hydrothermal alteration has measurably shifted the $^{41}K/^{39}K$ ratios of the rocks. The $^{41}K/^{39}K$ ratios were determined using an Isoprobe-P multicollector inductively coupled plasma mass spectrometer (MC-ICPMS) equipped with a collision and reaction cell that greatly reduces undesired Ar interferences. Isotope data are expressed as parts per thousand deviations from an estimate of bulk silicate earth (BSE): $\delta^{41/39}K = ((^{41}K/^{39}K)_{sample}/(^{41}K/^{39}K)_{BSE} - 1)*10^3$. In addition, elemental concentrations were measured for all samples using a Thermo Scientific Quadrupole ICPMS. Electron microprobe analyses were performed on the pillow basalt to investigate alteration textures. Details of our analytical procedures are given in *Methods*. Elemental data are provided in Table S1 and Figs. S1–S3, and back-scattered electron images in Figs. S4–S6.

Prior studies have established that the BOI ophiolite is an obducted fragment of ∼485 Ma oceanic crust (20–22) that closely resembles typical midocean ridge crust in its elemental composition and internal structure (23). However, the ophiolite most likely formed not at a midocean ridge, but at an oceanic spreading center located above a subduction zone (22, 24). Obduction occurred by ∼470 Ma, in association with the Taconic orogeny, as constrained by dating of minerals in the metamorphic aureole (25,

Significance

Elemental exchange between seawater and oceanic crust is important both in modulating the ionic composition of seawater over geologic time and in controlling the elemental and isotopic makeup of various solid-earth reservoirs. This study documents large and systematic variations in the K-isotope composition of oceanic crust that has been affected by seafloor hydrothermal alteration. These variations put constraints on the isotopic character of a fundamental flux of the marine K cycle: the hydrothermal flux. We also propose that these variations ought to be exploited in the future as an effective way of tracking oceanic crust as it is subducted into the mantle and sampled by various forms of volcanism.

Author contributions: S.B.J. designed research; C.A.P. performed research; C.A.P. analyzed data; K.W. contributed new reagents/analytic tools; and C.A.P. and S.B.J. wrote the paper.

The authors declare no conflict of interest.

This article is a PNAS Direct Submission.

[1]To whom correspondence should be addressed. Email: cparendo@fas.harvard.edu.

[2]Present address: Department of Earth and Planetary Sciences, Washington University, Saint Louis, MO 63130.

[3]Present address: McDonnell Center for the Space Sciences, Washington University, Saint Louis, MO 63130.

This article contains supporting information online at www.pnas.org/lookup/suppl/doi:10.1073/pnas.1609228114/-/DCSupplemental.

26). The subsequent history of this part of the continental margin includes events such as the Acadian and Alleghanian orogenies (27). The BMD massif of the BOI ophiolite is affected by some faults but is essentially intact (23), including in the area where our samples were obtained. The pseudostratigraphy in this area is complete, except that an estimated 400 m of the uppermost basalts may be missing (23). Neither obduction nor later tectonic events have left a discernable metamorphic overprint on the part of the ophiolite where our samples were taken (23).

The constituent rocks of the BMD massif have been variably metamorphosed in a manner consistent with hydrothermal processes. Metamorphic grade increases with depth in the stratigraphy, from prehnite–pumpellyite facies in the pillow basalts to amphibolite facies in the metagabbros (28). For a broader context, it is worth noting that, in the nearby North Arm massif, the topmost few hundred meters of the pillow basalts are preserved and are not metamorphosed to prehnite–pumpellyite grade (29). Pervasiveness of alteration—as manifest by the abundance of secondary minerals—decreases with depth (28). These features are similar to those documented in modern oceanic crust, where fluids infiltrate oceanic rocks of variable porosity in the presence of a geothermal gradient. The metamorphic textures of the BOI rocks have therefore been interpreted to be the result of hydrothermal alteration at the seafloor (23, 28).

The samples of this study were collected along a depth transect through the stratigraphy of the ophiolite, and include: a pillow basalt, two diabases from a sheeted dike complex, an oceanic plagiogranite, a hornblende gabbro, and an olivine gabbro. The samples have been described previously (30), and we supplement past observations with electron-microprobe analyses of the basalt sample. BMD-24 is a prehnite–pumpellyite facies metabasalt, with calcite veins, small crystals of plagioclase (partly replaced by albite), clinopyroxene, chlorite, and minor quartz. Potassium is concentrated in micron-sized patches, possibly of a micaceous phase, within the secondary albite (*Electron-Microprobe Analysis of Sample BMD-24*; Figs. S4–S7). BMD-10 is a greenschist facies metadiabase; it comes from a part of the sheeted dike complex where brecciation is extensive and interpreted to have resulted from the flow of supercritical seawater (28). BMD-12a is an amphibolite facies metadiabase that has been largely recrystallized. It consists predominantly of secondary amphibole and saussuritized plagioclase, with some chlorite and trace amounts of clinopyroxene. BMD-14 is an oceanic plagiogranite, located at the interface of the diabases and gabbros. BMD-8 is an amphibolite facies metagabbro with hornblende (presumably incorporating H_2O from seawater), epidote, and plagioclase. BMD-7 is a gabbro that is not significantly metamorphosed. It contains plagioclase with minor saussuritization, some secondary amphibole, and olivine with minor alteration to serpentine. Jacobsen and Wasserburg (30) also reported $^{87}Sr/^{86}Sr$ ratios for the samples. The basalt, diabases, plagiogranite, and hornblende gabbro have high $^{87}Sr/^{86}Sr$ values, interpreted to reflect extensive interaction with seawater. The olivine gabbro has $^{87}Sr/^{86}Sr$ near what is expected for unaltered material.

Our measurements show that $\delta^{41/39}K$ of the BOI samples ranges from −0.01 to +0.67‰ (Table 1; Fig. 1). The spread in these values is about an order of magnitude greater than analytical uncertainties. This variability in $\delta^{41/39}K$ of the ophiolite rocks is remarkable, as most terrestrial igneous rocks analyzed to date have $\delta^{41/39}K$ within ∼0.1‰ of the value estimated for BSE (18, 19). Among our samples, only BMD-7 (olivine gabbro) has $\delta^{41/39}K$ within error of the estimate for BSE. All other samples have significantly elevated $\delta^{41/39}K$. The basalt and diabase samples have $\delta^{41/39}K$ between +0.31 and +0.41‰. The plagiogranite has $\delta^{41/39}K$ of +0.67‰. The pattern in these data, in which all samples but the olivine gabbro are isotopically enriched, resembles the trend previously documented in $^{87}Sr/^{86}Sr$. Indeed, $\delta^{41/39}K$ and $^{87}Sr/^{86}Sr$ of the samples are correlated (Fig. 2*A*).

The most plausible explanation of these data is that $\delta^{41/39}K$ of the rocks varies as a result of chemical exchange between seawater and oceanic crust. This interpretation is consistent with the correlation between $\delta^{41/39}K$ and $^{87}Sr/^{86}Sr$, with the olivine gabbro's having $\delta^{41/39}K$ and $^{87}Sr/^{86}Sr$ characteristic of unaltered mafic rock, and with the relatively high $\delta^{41/39}K$ and $^{87}Sr/^{86}Sr$ values of the other samples. The $^{87}Sr/^{86}Sr$ of seawater for the time of interest is well constrained by measurements of early Ordovician sediments (31). However, $\delta^{41/39}K$ is only known for present-day seawater: $\delta^{41/39}K$ = +0.58‰. Although this value is likely to have fluctuated over time, it seems reasonable to assume that $\delta^{41/39}K$ of seawater has generally remained elevated relative to BSE. This assumption is supported by two analyses of evaporites from the late Permian, which have $\delta^{41/39}K$ of +0.51 and +0.71‰ (18). Thus, we use $\delta^{41/39}K$ of present-day seawater as a rough approximation for early Ordovician seawater.

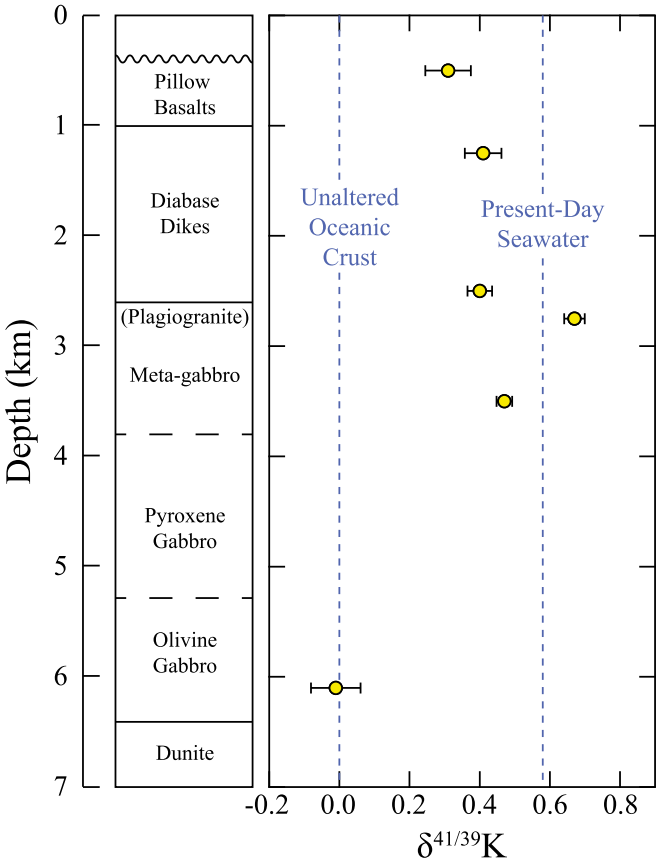

Fig. 1. The $\delta^{41/39}K$ values of the samples plotted as a function of depth within the ophiolite stratigraphy. The $\delta^{41/39}K$ estimate for BSE reported by ref. 18, which was based in part on analysis of a fresh MORB sample, is taken as the value for unaltered oceanic crust. Estimates of the $\delta^{41/39}K$ of present-day seawater are given in refs. 18 and 19.

Table 1. Potassium concentrations and isotope compositions of BOI samples

Sample	Rock type	[K] (ppm)	$\delta^{41/39}K_{BSE}$	2SE	*n*
BMD-24	Pillow basalt	1,220	0.31	0.065	4
BMD-10	Diabase	5,130	0.41	0.052	4
BMD-12a	Diabase	3,830	0.40	0.035	4
BMD-14	Plagiogranite	2,970	0.67	0.029	4
BMD-8	Hornblende gabbro	2,750	0.47	0.022	4
BMD-7	Olivine gabbro	373	−0.01	0.078	2

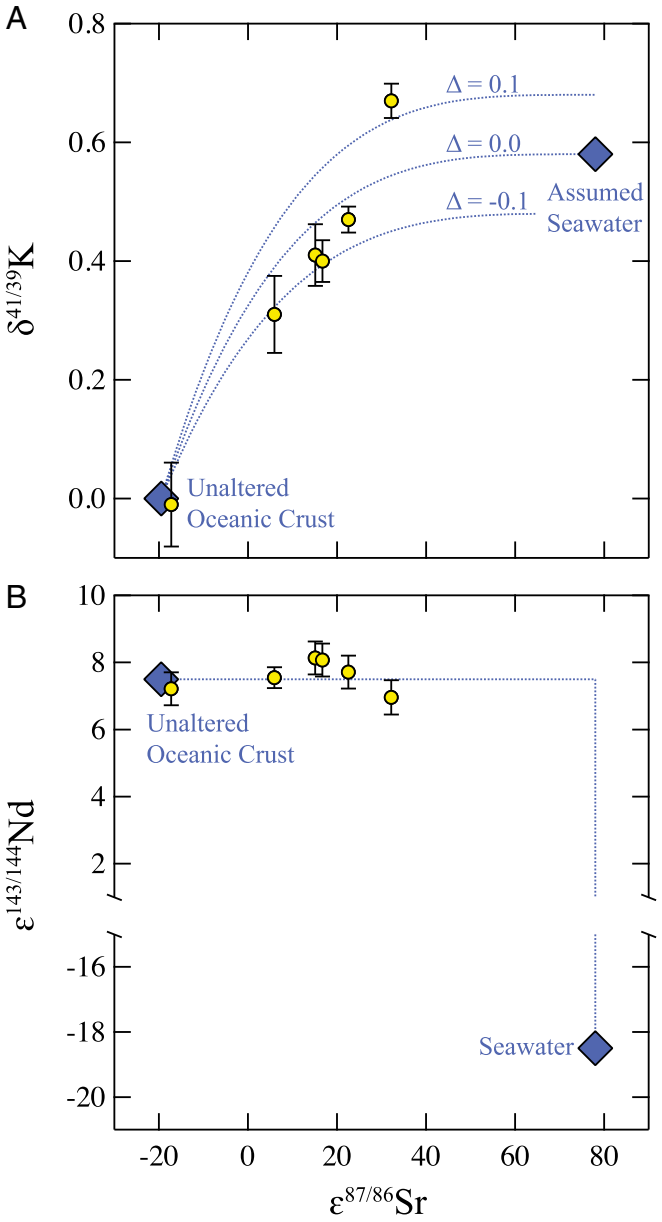

Fig. 2. The $\delta^{41/39}$K and $\varepsilon^{143/144}$Nd vs. $\varepsilon^{87/86}$Sr for BOI samples. Error bars on $\varepsilon^{87/86}$Sr data are smaller than the symbols. Model curves show expected trends for samples affected by seafloor hydrothermal alteration (*Modeling $\delta^{41/39}$K, $\varepsilon^{87/86}$Sr, and $\varepsilon^{143/144}$Nd Variations in AOC*). Data needed to estimate seawater $\varepsilon^{87/86}$Sr and $\varepsilon^{143/144}$Nd compositions are taken from refs. 31 and 40, respectively. There are no direct measurements for $\delta^{41/39}$K of early Ordovician seawater. We use the $\delta^{41/39}$K of present-day seawater as an approximation for the past, and note that this value is similar to values measured for two Permian sylvites (18). (*A*) $\delta^{41/39}$K covaries with $\varepsilon^{87/86}$Sr. Three model curves are drawn, corresponding to fractionation factors (Δ) between rock and seawater of −0.1, 0.0, and +0.1 ‰. (*B*) $\varepsilon^{143/144}$Nd does not covary significantly with $\varepsilon^{87/86}$Sr.

Having done so, we note that the samples plot along an array in the $\delta^{41/39}$K versus ^{87}Sr/^{86}Sr diagram between estimates for BSE and seawater (Fig. 2*A*).

Hydrothermal processes involving K vary in space and time. This is the case for modern oceanic crust, from which K is leached at higher temperatures (in the lower lithologies, near the ridge axis), and to which K is added at lower temperatures (in the upper lithologies, away from the ridge axis). Our pillow basalt sample (BMD-24) does not have higher K content than typical MORB. Nonetheless, imaging reveals that K is concentrated in a secondary phase (*Electron-Microprobe Analysis of Sample BMD-24* and Figs. S4–S7), implying mobile K was acquired from a fluid phase, as would be expected during low-temperature alteration. Deeper lithologies (diabases and metagabbros) may have been affected by alteration at higher temperatures, involving K loss, and subsequently at lower temperatures, involving K gain. We consider it likely that addition of K to the rocks during relatively low-temperature alteration is primarily responsible for imparting the $\delta^{41/39}$K effects observed here.

A limitation of this study is that it does not include samples from the uppermost ∼400 m of the pillow basalts, as this lithology is truncated in the BMD massif. It is typically observed in oceanic drill cores that by far the greatest enrichment in K content occurs in the shallowest part of the crust (7, 32), where rock is highly porous and most affected by interaction with seawater at low temperatures. A similar enrichment in the shallowest few hundred meters has been documented in the Troodos ophiolite (33). In contrast, a study of the Macquarie Island ophiolite estimated that K had been added in large quantities to greater depths (1–1.5 km) (34). Thus, there may be significant variability among sites in how K is distributed. Regardless, future work that characterizes the $\delta^{41/39}$K of the uppermost basalts, where much, if not most, of the total K in hydrothermally altered crust is stored, will be essential to producing a robust estimate of average $\delta^{41/39}$K for typical altered oceanic crust (AOC).

Rocks that have been variably affected by hydrothermal fluids ought to plot in a $\delta^{41/39}$K versus ^{87}Sr/^{86}Sr diagram along a trend line, the curvature of which depends on the relative susceptibility of each isotope system to alteration. Trend lines were calculated, using equations for open-system exchange (refs. 35 and 36), and are depicted in Fig. 2. These curves are based on reasonable parameter choices (*Modeling $\delta^{41/39}$K, $\varepsilon^{87/86}$Sr, and $\varepsilon^{143/144}$Nd Variations in AOC*). The value used for $\delta^{41/39}$K of ancient seawater is only provisional, and the magnitude of the fractionation effects associated with partitioning of K into alteration phases is not known. If the assumed value of $\delta^{41/39}$K for seawater is entertained, it appears that K added to oceanic crust during alteration has $\delta^{41/39}$K similar to the seawater reservoir from which it is derived; however, it is also possible that $\delta^{41/39}$K of early Ordovician seawater was markedly different from the present and/or that significant fractionation effects (on the order of tenths of a per mil) accompany the partitioning of K into secondary minerals. Despite uncertainties in the calculation, the agreement between the data and calculated trend lines illustrates that the $\delta^{41/39}$K and ^{87}Sr/^{86}Sr of the BOI samples are consistent with the interpretation that the observed isotopic variability results from seafloor hydrothermal alteration.

In reality, the processes that affected the various lithologies of the ophiolite must have been more complex than the simple open-system exchange model that we use. Fluid flow is likely to have been somewhat restricted, especially in the lower parts of the stratigraphy, below the volcanic zone. As a result, the fluids interacting with rocks at these depths would not simply have the chemical makeup of seawater but, rather, would have the composition of a seawater-derived fluid that had been modified during transport through shallower regions of the oceanic crust. Moreover, the plagiogranite may have formed by processes that influenced its isotopic composition in complex ways. Oceanic plagiogranites may be generated either by extreme differentiation of a tholeiitic parental magma or by hydrous partial melting of gabbro or diabase (37). In either of these scenarios, it is possible that the felsic magma bodies, from which plagiogranites crystallize, acquire distinct $\delta^{41/39}$K and ^{87}Sr/^{86}Sr as a result of processes such as wall rock assimilation or incorporation of hydrothermal fluids into the melts. In addition, mass-dependent fractionation of K isotopes may occur during some of the stages of plagiogranite formation. These factors may or may not be relevant to explaining how the plagiogranite came to have a $\delta^{41/39}$K that is

quite high. Nevertheless, the elevated $^{87}Sr/^{86}Sr$ of the plagiogranite (which does not reflect mass-dependent fractionation) points to incorporation of significant amounts of material derived from seawater, regardless of the exact process by which this occurred: water–rock exchange, assimilation of altered wall rock, or other. Studies performed with higher sampling density should be able to determine whether the processes that control $\delta^{41/39}K$ of plagiogranite are fundamentally different from those that control $\delta^{41/39}K$ of the mafic lithologies of oceanic crust.

The magnitude of variability in $\delta^{41/39}K$ and $^{87}Sr/^{86}Sr$ in the BOI samples cannot easily be attributed to other mechanisms, such as igneous fractionation effects or heterogeneity in the magma source materials. Partial melting is not expected to generate much $\delta^{41/39}K$ variability in magmatic products, because K is highly incompatible and partitions nearly quantitatively into melts. The $\delta^{41/39}K$ may be affected by fractional crystallization; however, most igneous rocks measured to date—including basalts, andesites, and granites—span a very limited range of only ∼0.1‰, suggesting that fractional crystallization of basaltic magmas does not commonly produce $\delta^{41/39}K$ effects of the size we report. Most importantly, the correlation between $\delta^{41/39}K$ and $^{87}Sr/^{86}Sr$ cannot be ascribed to an igneous fractionation mechanism, because $^{87}Sr/^{86}Sr$ values are not affected by mass-dependent fractionation processes.

We also consider it unlikely that source heterogeneity can explain the full range of variability in $\delta^{41/39}K$ and $^{87}Sr/^{86}Sr$. Like most well-known ophiolites, the BOI rocks have elemental compositions that show evidence of a subduction influence, consistent with a model in which the rocks formed at a spreading ridge situated above a subduction zone (refs. 22 and 24; *Elemental Compositions of BOI Samples*). Although incorporation of variable amounts of a subduction component into the magmas may have occurred, there are multiple reasons to doubt that this is the primary driver of the observed isotopic variability. (*i*) The $^{87}Sr/^{86}Sr$ ratios of the BOI rocks are elevated to a greater extent than what is generally seen in suprasubduction volcanic products, such as island–arc rocks or back-arc–basin basalts. (*ii*) Variable incorporation of a subduction component might be expected to result in variations in $^{143}Nd/^{144}Nd$ coupled to those in $\delta^{41/39}K$ and $^{87}Sr/^{86}Sr$, but $^{143}Nd/^{144}Nd$ is essentially constant among the samples (Fig. 2*B*). Also, the age-corrected $^{143}Nd/^{144}Nd$ ratios of the samples are relatively high. Lavas that erupted in settings such as island arcs may show a range in $^{87}Sr/^{86}Sr$ with only modest variation in $^{143}Nd/^{144}Nd$ as a result of a subduction influence, but these volcanic products also tend to have lower $^{143}Nd/^{144}Nd$. In this way, the $^{143}Nd/^{144}Nd$ ratios support a common—or, at least, similar—source material for all of the rocks sampled, because $^{143}Nd/^{144}Nd$ is sensitive to mantle heterogeneity but is basically insensitive to hydrothermal alteration effects. (*iii*) The $\delta^{41/39}K$ values of the BOI rocks are enriched more than essentially all other common igneous rocks analyzed to date, including one arc andesite—albeit the existing $\delta^{41/39}K$ dataset is small. (*iv*) Mixing with a subduction component would not be expected to generate any simple relationships between $\delta^{41/39}K$ and $^{87}Sr/^{86}Sr$ values and depth, yet $\delta^{41/39}K$ values are identical to BSE at depth and different from BSE in the upper stratigraphy (Fig. 1).

The high $\delta^{41/39}K$ of the BOI samples indicates that hydrothermally altered crust is likely to have $\delta^{41/39}K$ that is elevated in comparison with BSE (which is estimated to have $\delta^{41/39}K = 0.0‰$). However, more research is needed to determine how representative these samples are of typical altered oceanic crust. The data of this study show that the BOI ophiolite has high $\delta^{41/39}K$ at least in regions below ∼400 m. The basalt and diabase samples have $\delta^{41/39}K$ values that range between +0.31 and +0.41‰. It remains to be tested whether these values are characteristic of the shallowest crust, where a large amount of K is stored. The plagiogranite has higher $\delta^{41/39}K$, but this lithology is a minor constituent by mass of the ophiolite. Another consideration is that oceanic crust generated in suprasubduction zone settings appears generally to be more extensively altered than crust formed at midocean ridges (38, 39). Accordingly, the BOI ophiolite may have been altered more thoroughly or to a greater depth than typical AOC. On the other hand, the processes of alteration—and the direction of chemical and isotopic effects—appear to be broadly similar in both types of tectonic setting (38). Also, the basalt and diabase samples of this study have $^{87}Sr/^{86}Sr$ ratios that are comparable to those of AOC obtained in drill cores, so these samples may in fact be reasonable proxies for AOC. Going forward, there will be value in examining $\delta^{41/39}K$ at higher resolution in ophiolitic and drill-cored oceanic crust from diverse locations. This will allow a more thorough assessment of how $\delta^{41/39}K$ effects depend upon factors such as depth below seafloor, grade of metamorphism, and tectonic setting. Based on the data from the BOI ophiolite, it appears that altered material tends to have high $\delta^{41/39}K$, but a robust estimate of the magnitude of this effect in average AOC is not yet possible.

If elevated $\delta^{41/39}K$ is a feature of AOC as this study suggests, then K isotopes will be useful as a tracer of AOC recycling. The isotopic contrast in $\delta^{41/39}K$ between AOC and the mantle ($\delta^{41/39}K$ ∼0.0‰) is potentially large. Moreover, the concentration of K in AOC is many times greater than in the mantle. As a result, addition of even small amounts of subducted AOC material to the mantle is likely to generate large $\delta^{41/39}K$ effects in the resultant mixtures. All of this implies that, in the future, $\delta^{41/39}K$ may be used to track the fate of subducted material as it is mixed into the mantle and sampled by island–arc, ocean–island, and midocean-ridge volcanism.

A distinctive $\delta^{41/39}K$ of AOC could also be useful for establishing whether certain old rocks that have undergone complex deformation or metamorphism are, in fact, ancient fragments of oceanic crust. The effectiveness of K isotopes toward this purpose would depend on multiple factors, one being whether extensive interaction between the rocks and continental-derived fluids had occurred.

Last, as the $\delta^{41/39}K$ of AOC is constrained, it will be possible to better characterize the hydrothermal flux of K between oceanic crust and seawater, which is an important flux for the marine K cycle. Determining the isotope effects associated with this and other fluxes is critical for constructing an improved mass balance for the sources and sinks of K to and from the oceans. Potassium-isotope data therefore fit into a long-term project of constraining the rates of processes such as hydrothermal alteration, weathering, and reverse weathering that are known to modulate seawater chemistry over geologic time.

Methods

Sample Dissolution and Chromatographic Separation of K. Samples were powdered and dissolved in a multistep process. For each sample, aliquots of 20–100 mg of rock powder were used. First, powders were put into digestion vessels with a mix of concentrated acids (0.5 mL HF, 2 mL HNO_3, and 1 mL HCl), with HF included to break Si–O bonds, and were heated by a CEM Microwave Accelerated Reaction System to 200 °C for 1.5 h. Second, the solutions were dried down, redissolved in a different mix of acids (0.5 HNO_3, 1.5 HCL, 1 mL H_2O) to facilitate dissociation of CaF_2 residues, and heated in the same manner as before. Third, samples were dried down and redissolved in acids (0.5 HNO_3, 1.5 HCL, 1 mL H_2O) without microwave heating. Finally, samples were dried down and redissolved in 1 mL of 0.5 N HNO_3 in preparation for chromatography.

The two-step procedure used for chromatography has been described in ref. 18. For the first step, we used quartz-glass columns with 1-cm inner diameter, filled with Bio-Rad AG50W-X8 (100–200 mesh) cation exchange resin. The resin volume is 13 mL, as measured when it is saturated in 4N HNO_3. Before each use, columns were cleaned with 300 mL 4 N HCl. Some Milli-Q water was added to flush out the HCl, and then columns were conditioned with 50 mL of 0.5 N HNO_3. Samples were loaded in 1 mL 0.5 N HNO_3 and eluted with 340 mL of 0.5 N HNO_3, and the K-containing cut at 160–340 mL was collected. The solution was dried down. For the second step, we used quartz-glass columns with 0.4-cm inner diameter and 1.6 mL of the same resin. Columns were cleaned with 100 mL 4 N HCl, flushed with 10 mL Milli-Q water, and conditioned with 20 mL 0.5 N HNO_3.

Samples were loaded in 0.5 mL 0.5 N HNO_3 and eluted with 47 mL 0.5 N HNO_3. The cut at 28–47 mL was collected. The solutions were dried down and redissolved in 0.32 N HNO_3.

Measurement of $^{41}K/^{39}K$ by Mass Spectrometry. Our method for measuring $^{41}K/^{39}K$ ratios has been described in ref. 18. Analyses were performed with a GV Instruments IsoProbe-P MC-ICPMS. The instrument is equipped with a hexapole collision and reaction cell, which greatly reduces Ar-hydride interferences (i.e., $^{40}Ar^{1}H$ and $^{38}Ar^{1}H$). Analyses of sample solutions were bracketed by analyses of blank (0.32 N HNO_3) and standard, to conduct blank subtractions and to express $^{41}K/^{39}K$ ratios relative to our reference material. The laboratory standard is Merck KGaA Suprapur high-purity potassium nitrate (KNO_3). An estimate of BSE relative to this standard was provided by ref. 18, which has made it possible for us to express the data of this study relative to the BSE estimate. That is, we initially generated $^{41}K/^{39}K$ values relative to the laboratory standard, which we can express in delta notation as follows: $\delta^{41/39}K_{relative\_to\_lab\_standard} = (((^{41}K/^{39}K)_{sample}/(^{41}K/^{39}K)_{lab\_standard} - 1)*10^3$. To express our data relative to the BSE estimate of ref. 18, we used the following conversion: $\delta^{41/39}K_{relative\_to\_BSE} = 1.000479*\delta^{41/39}K_{relative\_to\_lab\_standard} + 0.479230$. Repeat analyses of standards and samples during the course of this project demonstrated an external reproducibility of ∼0.07 (2SD). A single measurement in this study consists of running a sample solution, bracketed by a standard solution, 5–6 times over the course of some hours. Replicate measurements allowed us to determine $\delta^{41/39}K$ of samples to precisions typically of ∼0.035 (2SE).

Measurement of Elemental Concentrations by Mass Spectrometry. Major and trace elements were measured using a Thermo Scientific Quadrupole ICPMS. Calibration curves, relating signal intensities to elemental concentrations, were generated by analyzing United States Geological Survey standards BCR-1, BHVO-1, and AGV-1.

ACKNOWLEDGMENTS. Editorial handling by David Walker and helpful comments from two reviewers are gratefully acknowledged. We thank Michail I. Pataev for operating the electron microprobe and assisting in the generation and interpretation of petrographic images. This work was funded by National Science Foundation Grant EAR-1144727 and NASA Grant NNX15AH66G.

1. Elderfield H, Schultz A (1996) Mid-ocean ridge hydrothermal fluxes and the chemical composition of the ocean. *Annu Rev Earth Planet Sci* 24:191–224.
2. Nielsen SG, et al. (2006) Hydrothermal fluid fluxes calculated from the isotopic mass balance of thallium in the ocean crust. *Earth Planet Sci Lett* 251(1-2):120–133.
3. Chen YJ, Morgan JP (1996) The effects of spreading rate, the magma budget, and the geometry of magma emplacement on the axial heat flux at mid-ocean ridges. *J Geophys Res Solid Earth* 101(B5):11475–11482.
4. Dasch EJ, Hedge CE, Dymond J (1973) Effect of sea-water interaction on strontium isotope composition of deep-sea basalts. *Earth Planet Sci Lett* 19(2):177–183.
5. Muehlenbachs K, Clayton RN (1976) Oxygen isotope composition of oceanic-crust and its bearing on seawater. *J Geophys Res* 81(23):4365–4369.
6. Hart S, Erlank A, Kable E (1974) Sea floor basalt alteration: Some chemical and Sr isotopic effects. *Contrib Mineral Petrol* 44(3):219–230.
7. Staudigel H (2003) Hydrothermal alteration processes in the oceanic crust. *Treatise on Geochemistry*, ed Rudnick RL (Elsevier, New York), Vol 3, pp 511–535.
8. Staudigel H, Davies G, Hart SR, Marchant K, Smith BM (1995) Large scale isotopic Sr, Nd and O isotopic anatomy of altered oceanic crust: DSDP/ODP sites417/418. *Earth Planet Sci Lett* 130(1):169–185.
9. Eiler JM (2001) Oxygen isotope variations of basaltic lavas and upper mantle rocks. *Rev Mineral Geochem* 43(1):319–364.
10. Hawkesworth C, Gallagher K, Hergt J, McDermott F (1993) Mantle and slab contribution in arc magmas. *Annu Rev Earth Planet Sci* 21:175–204.
11. Cohen R, O'Nions RK (1982) The lead, neodymium and strontium isotopic structure of ocean ridge basalts. *J Petrol* 23(3):299–324.
12. Edmond JM, et al. (1979) Ridge crest hydrothermal activity and the balances of the major and minor elements in the ocean: The Galapagos data. *Earth Planet Sci Lett* 46(1):1–18.
13. Von Damm K, et al. (1985) Chemistry of submarine hydrothermal solutions at 21° N, East Pacific Rise. *Geochim Cosmochim Acta* 49(11):2197–2220.
14. Hart SR, Staudigel H (1982) The control of alkalies and uranium in seawater by ocean crust alteration. *Earth Planet Sci Lett* 58(2):202–212.
15. Kelley KA, Plank T, Ludden J, Staudigel H (2003) Composition of altered oceanic crust at ODP Sites 801 and 1149. *Geochem Geophys Geosyst*, 10.1029/2002GC000435.
16. Wheat CG, Mottl MJ (2000) Composition of pore and spring waters from Baby Bare: Global implications of geochemical fluxes from a ridge flank hydrothermal system. *Geochim Cosmochim Acta* 64(4):629–642.
17. Seyfried W, Bischoff J (1979) Low temperature basalt alteration by sea water: An experimental study at 70 C and 150 C. *Geochim Cosmochim Acta* 43(12):1937–1947.
18. Wang K, Jacobsen SB (2016) An estimate of the Bulk Silicate Earth potassium isotopic composition based on MC-ICPMS measurements of basalts. *Geochim Cosmochim Acta* 178:223–232.
19. Li W, Beard BL, Li S (2016) Precise measurement of stable potassium isotope ratios using a single focusing collision cell multi-collector ICP-MS. *J Anal At Spectrom* 31(4): 1023–1029.
20. Church Wt, Stevens R (1971) Early Paleozoic ophiolite complexes of the Newfoundland Appalachians as mantle-oceanic crust sequences. *J Geophys Res* 76(5):1460–1466.
21. Dunning G, Krogh T (1985) Geochronology of ophiolites of the Newfoundland Appalachians. *Can J Earth Sci* 22(11):1659–1670.
22. Jenner G, Dunning G, Malpas J, Brown M, Brace T (1991) Bay of Islands and Little Port complexes, revisited: age, geochemical and isotopic evidence confirm suprasubduction-zone origin. *Can J Earth Sci* 28(10):1635–1652.
23. Salisbury MH, Christensen NI (1978) The seismic velocity structure of a traverse through the Bay of Islands ophiolite complex, Newfoundland, an exposure of oceanic crust and upper mantle. *J Geophys Res Solid Earth* 83(B2):805–817.
24. Elthon D (1991) Geochemical evidence for formation of the Bay of Islands ophiolite above a subduction zone. *Nature* 354:140–143.
25. Dallmeyer R, Williams H (1975) 40Ar/39Ar ages from the Bay of Islands metamorphic aureole: Their bearing on the timing of Ordovician ophiolite obduction. *Can J Earth Sci* 12(9):1685–1690.
26. Cawood PA, Suhr G (1992) Generation and obduction of ophiolites: Constraints from the Bay of Islands Complex, western Newfoundland. *Tectonics* 11(4):884–897.
27. Williams H (1979) Appalachian orogen in Canada. *Can J Earth Sci* 16(3):792–807.
28. Williams H, Malpas J (1972) Sheeted dikes and brecciated dike rocks within transported igneous complexes Bay of Islands, Western Newfoundland. *Can J Earth Sci* 9(9):1216–1229.
29. Christensen NI, Salisbury MH (1979) Seismic anisotropy in the oceanic upper mantle: Evidence from the Bay of Islands ophiolite complex. *J Geophys Res Solid Earth* 84(B9): 4601–4610.
30. Jacobsen SB, Wasserburg G (1979) Nd and Sr isotopic study of the Bay of Islands ophiolite complex and the evolution of the source of midocean ridge basalts. *J Geophys Res Solid Earth* 84(B13):7429–7445.
31. Ebneth S, Shields GA, Veizer J, Miller J, Shergold J (2001) High-resolution strontium isotope stratigraphy across the Cambrian-Ordovician transition. *Geochim Cosmochim Acta* 65(14):2273–2292.
32. Alt JC (1995) Subseafloor processes in mid-ocean ridge hydrothermal systems. *Seafloor Hydrothermal Systems: Physical, Chemical, Biological, and Geological Interactions*, eds Humphris SE, Zierenberg RA, Mullineaux LS, Thomson RE (American Geophysical Union, Washington, DC), pp 85–114.
33. Bednarz U, Schmincke H-U (1989) Mass transfer during sub-seafloor alteration of the upper Troodos crust (Cyprus). *Contrib Mineral Petrol* 102(1):93–101.
34. Coggon RM, et al. (2016) Hydrothermal contributions to global biogeochemical cycles: Insights from the Macquarie Island ophiolite. *Lithos* 264:329–347.
35. Banner JL, Hanson GN (1990) Calculation of simultaneous isotopic and trace element variations during water-rock interaction with applications to carbonate diagenesis. *Geochim Cosmochim Acta* 54(11):3123–3137.
36. Jacobsen SB, Kaufman AJ (1999) The Sr, C and O isotopic evolution of Neoproterozoic seawater. *Chem Geol* 161(1):37–57.
37. Koepke J, Berndt J, Feig ST, Holtz F (2007) The formation of SiO2-rich melts within the deep oceanic crust by hydrous partial melting of gabbros. *Contrib Mineral Petrol* 153(1):67–84.
38. Alt JC, Teagle DA, Brewer T, Shanks WC, Halliday A (1998) Alteration and mineralization of an oceanic forearc and the ophiolite-ocean crust analogy. *J Geophys Res Solid Earth* 103(B6):12365–12380.
39. Alt JC, Teagle DA (2000) Hydrothermal alteration and fluid fluxes in ophiolites and oceanic crust. *Geol Soc Am, Spec Pap* 349:273–282.
40. Wright CA, Barnes CR, Jacobsen SB (2002) Neodymium isotopic composition of Ordovician conodonts as a seawater proxy: Testing paleogeography. *Geochem Geophys Geosyst*, 10.1029/2001GC000195.
41. Villa I, De Bievre P, Holden N, Renne P (2015) IUPAC-IUGS recommendation on the half life of 87 Rb. *Geochim Cosmochim Acta* 164:382–385.
42. Lugmair G, Marti K (1978) Lunar initial 143 Nd/144 Nd: Differential evolution of the lunar crust and mantle. *Earth Planet Sci Lett* 39(3):349–357.
43. DePaolo D, Wasserburg G (1976) Inferences about magma sources and mantle structure from variations of 143Nd/144Nd. *Geophys Res Lett* 3(12):743–746.
44. Papanastassiou DA, Wasserburg G (1968) Initial strontium isotopic abundances and the resolution of small time differences in the formation of planetary objects. *Earth Planet Sci Lett* 5:361–376.
45. Jacobsen SB, Wasserburg G (1980) Sm-Nd isotopic evolution of chondrites. *Earth Planet Sci Lett* 50(1):139–155.
46. Jacobsen S, Wasserburg G (1984) Sm-Nd isotopic evolution of chondrites and achondrites, II. *Earth Planet Sci Lett* 67(2):137–150.
47. Horita J, Zimmermann H, Holland HD (2002) Chemical evolution of seawater during the Phanerozoic: Implications from the record of marine evaporites. *Geochim Cosmochim Acta* 66(21):3733–3756.
48. Vollstaedt H, et al. (2014) The Phanerozoic δ 88/86 Sr record of seawater: New constraints on past changes in oceanic carbonate fluxes. *Geochim Cosmochim Acta* 128:249–265.
49. Steuber T, Veizer J (2002) Phanerozoic record of plate tectonic control of seawater chemistry and carbonate sedimentation. *Geology* 30(12):1123–1126.
50. McDonough WF, Sun S-S (1995) The composition of the Earth. *Chem Geol* 120(3): 223–253.
51. Gale A, Dalton CA, Langmuir CH, Su Y, Schilling JG (2013) The mean composition of ocean ridge basalts. *Geochem Geophys Geosyst* 14(3):489–518.

Supporting Information

Parendo et al. 10.1073/pnas.1609228114

Age-Corrected $\varepsilon^{87/86}$Sr and $\varepsilon^{143/144}$Nd Values

All ε values in this paper are calculated for an age of 485 Ma, which is the current best estimate for the age of crystallization of rocks from the Blow Me Down massif of the BOI Ophiolite (21, 22). That is, $\varepsilon^{87/86}\mathrm{Sr} = (((^{87}\mathrm{Sr}/^{86}\mathrm{Sr})_{\mathrm{sample}}/(^{87}\mathrm{Sr}/^{86}\mathrm{Sr})_{\mathrm{BSE}} - 1)*10^4$, where the $^{87}\mathrm{Sr}/^{86}\mathrm{Sr}$ ratios of the sample and reference reservoir are corrected for mass-dependent fractionation, and are corrected for radiogenic ingrowth. Similarly, $\varepsilon^{143/144}\mathrm{Nd} = ((^{143}\mathrm{Nd}/^{144}\mathrm{Nd})_{\mathrm{sample}}/(^{143}\mathrm{Nd}/^{144}\mathrm{Nd})_{\mathrm{CHUR}} - 1)*10^4$, where the $^{143}\mathrm{Nd}/^{144}\mathrm{Nd}$ ratios are corrected for fractionation and age. The decay constants used are $\lambda_{87\mathrm{Rb}} = 1.3972*10^{-11}\ \mathrm{y}^{-1}$ (41), and $\lambda_{147\mathrm{Sm}} = 6.54*10^{-12}\ \mathrm{y}^{-1}$ (42). The parameters used to define the BSE reservoir for the Rb–Sr system are $(^{87}\mathrm{Sr}/^{86}\mathrm{Sr})_{\mathrm{BSE}} = 0.7045$ at present day (43), and $(^{87}\mathrm{Rb}/^{86}\mathrm{Sr})_{\mathrm{BSE}} = 0.08384$ at present day—the latter value calculated from the present-day $(^{87}\mathrm{Sr}/^{86}\mathrm{Sr})_{\mathrm{BSE}}$, the initial solar system $^{87}\mathrm{Sr}/^{86}\mathrm{Sr}$ estimate of ref. 44, and a solar system age of 4.567 Ga. The parameters used to define the chondritic uniform reservoir (CHUR) for the Sm–Nd system are $(^{143}\mathrm{Nd}/^{144}\mathrm{Nd})_{\mathrm{CHUR}} = 0.511847$ at present day for a $^{146}\mathrm{Nd}/^{144}\mathrm{Nd}$ normalizing ratio of 0.724134 that was used by ref. 30, and $(^{147}\mathrm{Sm}/^{144}\mathrm{Nd})_{\mathrm{CHUR}} = 0.1967$ at present day (45, 46).

Modeling $\delta^{41/39}$K, $\varepsilon^{87/86}$Sr, and $\varepsilon^{143/144}$Nd Variations in AOC

Our approach to calculating the effect of hydrothermal alteration on the rocks is to use an open-system water–rock interaction model, as described by ref. 36. The model is premised on a system in which fresh seawater continually flows through and chemically equilibrates with porous rock, causing the rock to be altered incrementally over time. Ultimately, the degree of alteration of the rock can be expressed as a function of the integrated flux of water through the rock—a parameter called the water–rock ratio. Written using δ notation, appropriate for the stable-isotope $^{41}\mathrm{K}/^{39}\mathrm{K}$ system, the model equation is as follows:

$$\delta^r = \frac{\left(\frac{C^{r0}}{C^{w0}}\right)\delta^{r0} + D\left(e^{\eta/D} - 1\right)(\Delta + \delta^{w0})}{\left(\frac{C^{r0}}{C^{w0}}\right) + D(e^{\eta/D} - 1)}.$$

Here, the isotopic composition of an element in the rock, δ^r, is expressed in terms of a distribution coefficient, D; an isotopic fractionation factor, Δ; initial concentrations of the element in the rock and fluid, C^{r0} and C^{w0}; initial isotopic compositions of the rock and fluid, δ^{r0} and δ^{w0}; and the water–rock ratio, η. The equation can also be written using ε notation, which is appropriate for the radiogenic-isotope $^{87}\mathrm{Sr}/^{86}\mathrm{Sr}$ and $^{143}\mathrm{Nd}/^{144}\mathrm{Nd}$ systems:

$$\varepsilon^r = \frac{\left(\frac{C^{r0}}{C^{w0}}\right)\varepsilon^{r0} + D\delta^{w0}\left(e^{\eta/D} - 1\right)}{\left(\frac{C^{r0}}{C^{w0}}\right) + D(e^{\eta/D} - 1)}.$$

Note that this latter expression is identical to the former, except for the use of ε notation and the necessary omission of the fractionation factor term. Thus, equations can be written for each of the three isotope systems: $\delta^{41/39}$K, $\varepsilon^{87/86}$Sr, and $\varepsilon^{143/144}$Nd. By combining any two of these equations, and in the process eliminating the η term, it is possible to express the isotopic composition of any one element as a function of the isotopic composition of any other element in the rock (e.g., $\delta^{41/39}$K as a function of $\varepsilon^{87/86}$Sr, as in Fig. 2*A*).

The parameter values we used for calculating the model curves in Fig. 2 are described below. The calculation is generally less sensitive to the parameters related to concentration (C^{r0}, C^{w0}, D) than to those pertaining to isotopic composition. We therefore make a simplifying assumption that the present-day concentrations of K, Sr, and Nd in the rocks are the same as the initial concentrations. This assumption determines the term C^{r0} and defines $D = C^{r0}/C^{w0}$. This assumption is, of course, not strictly true, especially for K, of which there is probably a net addition to the rock. However, generating the model curves under different reasonable assumptions—e.g., some increase in K content with alteration—does not significantly change our conclusions. Moreover, it would be difficult to estimate initial K or Sr concentrations for the BOI rocks, because they formed not at a typical midocean ridge, but rather in a suprasubduction zone setting.

Potassium.

K^{r0}	K^{w0}	D_K	$\delta^{r0}_{41/39}$	$\delta^{w0}_{41/39}$	Δ^{r-w}
3,350	380	K^{r0}/K^{w0}	0	0.58	0.0–0.2

The K content of the BOI samples varies. We use an intermediate value of 3,350 ppm. According to fluid inclusion studies, the K concentration of seawater may have been similar at 485 Ma to its present-day value of 380 ppm (47). Here, $\delta^{r0}_{41/39} = 0$ is the value of BSE, the estimate of which is based in part on analyses of a fresh MORB sample (18). We base $\delta^{w0}_{41/39}$ on the $\delta^{41/39}$K value of present-day seawater. The fractionation factor term is not constrained. We plot contours for values ranging from 0.0 to 0.2, as these are plausible and are consistent with our data.

Strontium.

Sr^{r0}	Sr^{w0}	D_{Sr}	$\varepsilon^{r0}_{87/86}$	$\varepsilon^{w0}_{87/86}$	Δ^{r-w}
260	8	Sr^{r0}/Sr^{w0}	−19.5	78	n.a.

The Sr content of the samples varies, though within a more limited range than does K. We use an intermediate value of 260 ppm. We use the present-day seawater Sr concentration of 8 ppm. Some studies have concluded that the Sr concentration of seawater was likely higher in the early Ordovician than at present (48), as a result of a lesser Sr sink during an interval of calcitic seas (49). However, using a higher Sr concentration in our calculation, by a factor of 2, does not change the model curves so much as to alter the conclusions of this paper. Here, $\varepsilon^{r0}_{87/86}$ is taken to be −19.5, about the most negative $\varepsilon^{87/86}$Sr values measured in the BOI rocks (30). Also, $\varepsilon^{w0}_{87/86}$ is based on the data of ref. 31.

Neodymium.

Nd^{r0}	Nd^{w0}	D_{Nd}	$\varepsilon^{r0}_{143/144}$	$\varepsilon^{w0}_{143/144}$	Δ^{r-w}
8	$3*10^{-6}$	Nd^{r0}/Nd^{w0}	7.5	−18.5	n.a.

We use an intermediate value of 8 ppm for the Nd content of the rock, and the present-day Nd concentration of seawater as an estimate for the past. Here, $\varepsilon^{r0}_{143/144} = 7.5$ is around the average of the BOI samples; $\varepsilon^{w0}_{143/144} = -18.5$ is based on analyses of two early-Ordovician conodonts in Newfoundland (40).

Elemental Compositions of BOI Samples

All elemental data are included in Table S1. Additionally, elemental data are illustrated in several figures. Data for the diabases and basalts are plotted in order of compatibility in Figs. S1 and S2, normalized to the BSE estimate of ref. 50 and the mean N-MORB estimate of ref. 51. These plots depict general similarity between the BOI samples and N-MORB, but also deviations of the BOI samples from the N-MORB trend among mobile elements. We note that these deviations are likely a result of two factors: (*i*) a subduction-zone influence, and (*ii*) hydrothermal alteration. Data for generally immobile elements for the diabases and basalts are plotted in Fig. S3. This plot indicates the presence of Nb and Ta depletions in at sample BMD-24, and very small Ta depletions in BMD-10 and -12a. This is in accord with previous studies that documented Nb and Ta depletions in the BOI ophiolite and interpreted these as the result of a subduction-zone influence (22, 24).

Electron-Microprobe Analysis of Sample BMD-24

Elemental mapping and spot analyses were performed by electron-microprobe on the pillow basalt sample (BMD-24). Figs. S4–S6 document some of the textures and secondary mineralogy of the sample. K is largely concentrated in patches of Na-rich feldspar (in some places, pure albite), which has replaced plagioclase in much of the rock. These patches are quite small (micron scale) so that it is difficult to identify the phase with certainty. Spot analyses (which sample the patches and surrounding material) indicate that it is a silicate, which could plausibly be a K feldspar or another K-bearing mineral. The K-rich patches coincide with indentations in the polished rock surface, so we infer that the phase is relatively soft. On this basis, we consider it probable that the patches consist of one or more fine-grained micaceous minerals (i.e., clays).

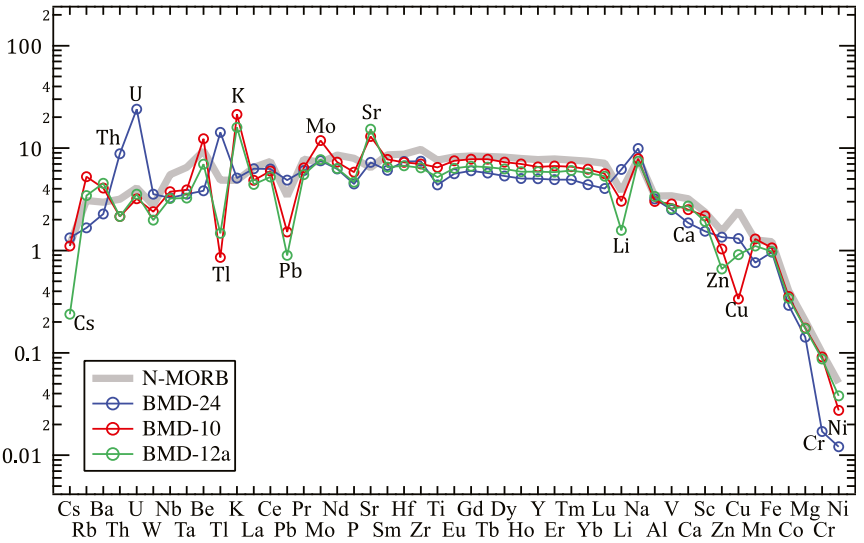

Fig. S1. Elemental abundances of samples normalized to BSE of ref. 50.

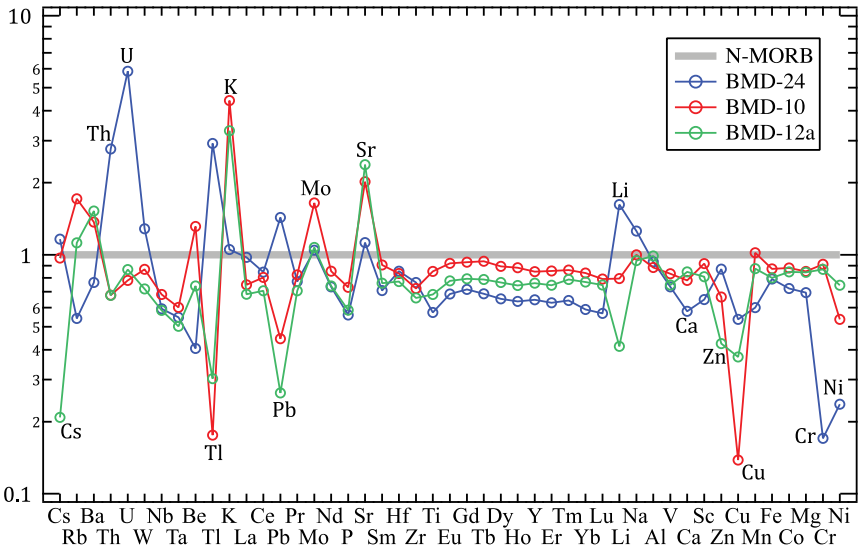

Fig. S2. Elemental abundances of samples normalized to N-MORB of ref. 51.

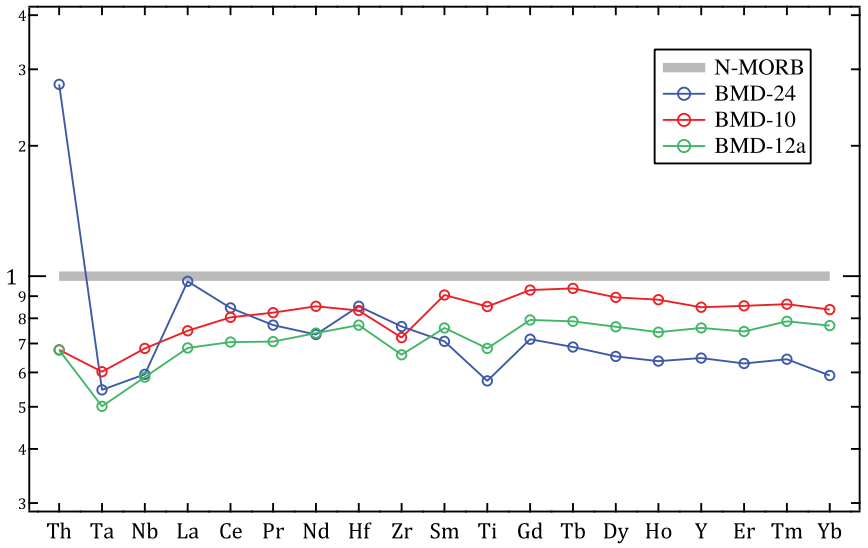

Fig. S3. Immobile elemental abundances of samples normalized to N-MORB of ref. 51.

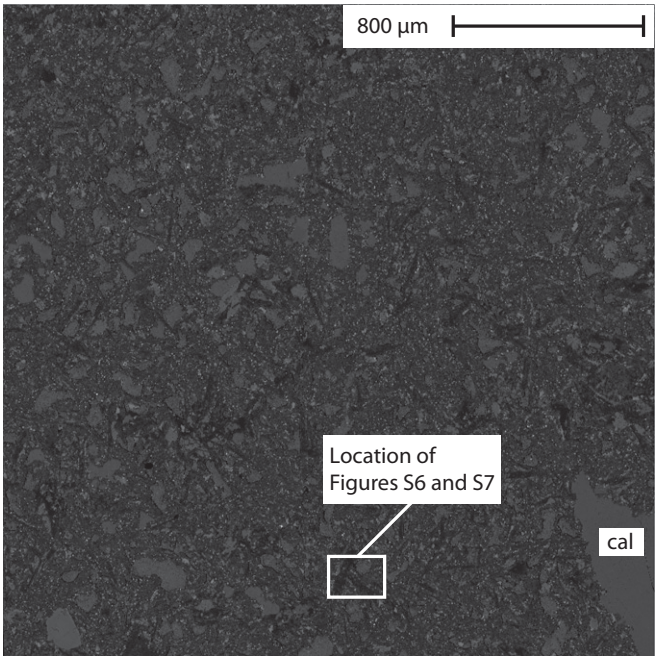

Fig. S4. Backscattered electron image of sample BMD-24, showing: (*i*) overview of the texture of the pillow basalt and (*ii*) secondary calcite (cal).

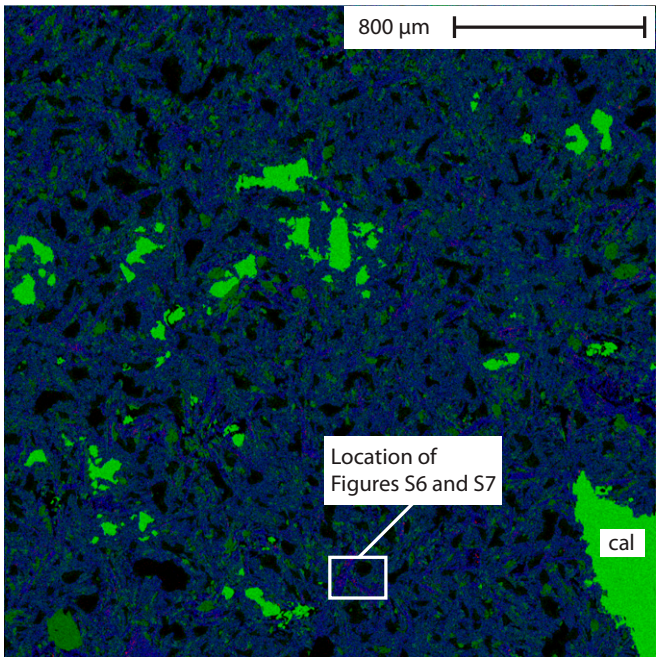

Fig. S5. Combined elemental map of BMD-24 in K (red), Ca, (green), and Na (blue) K_α X-rays. K is concentrated in small patches, which are easier to see at greater magnification, such as in Fig. S7.

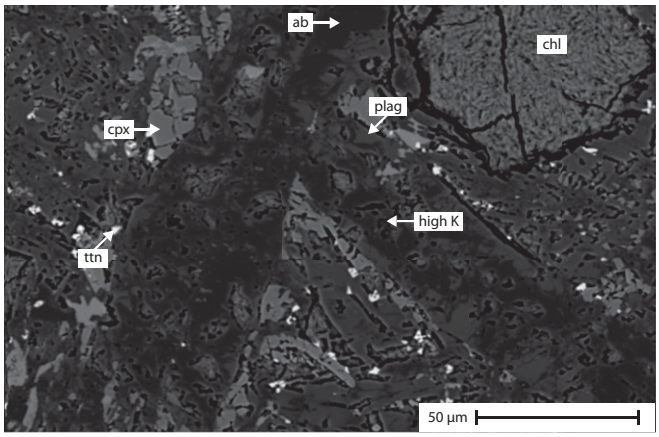

Fig. S6. Backscattered electron image of region enclosed in Figs. S4 and S5. Abbreviated mineral names are: plag, plagioclase; ab, albite; cpx, clinopyroxene; chl, chlorite; ttn, titanite. Two large laths of primary plagioclase associated with smaller grains of primary clinopyroxene and a large grain of secondary chlorite. Plagioclase is mostly replaced by secondary albite, which encloses numerous tiny patches with high K content (high-K). These patches correspond to areas where polishing has resulted in plucking out of soft materials. Fine-grained areas in the upper left region and in between the chlorite and plagioclase most likely represent recrystallized mesostasis.

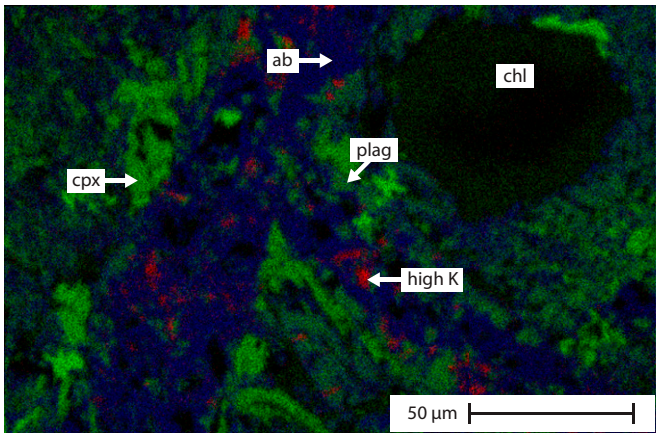

Fig. S7. Combined elemental map of BMD-24 in K (red), Ca, (green), and Na (blue) K_α X-rays. K is concentrated in small patches (red) within secondary Na-feldspar (blue), which has largely replaced plagioclase (green). Clinopyroxene appears as a brighter shade of green. Note that the field of view in Fig. S6 is shifted slightly compared within Fig. S5.

Table S1. Elemental compositions of samples

Element	BMD-24	BMD-10	BMD-12a	BMD-14	BMD-8	BMD-7
Li	9.88	4.85	2.52	0.53	2.09	1.04
Be	0.260	0.840	0.473	1.410	0.858	0.064
B	5.74	7.76	7.42	5.52	6.96	2.40
Na	26,400	21,000	19,800	39,900	32,900	9,690
Mg	32,500	39,900	39,400	2,060	22,300	55,300
Al	74,800	70,700	79,100	70,800	88,600	84,100
K	1,220	5,130	3,830	2,970	2,750	373
Ca	47,000	63,400	68,800	11,800	55,900	81,700
Sc	24.9	35.3	31.1	8.8	23.3	22.9
Ti	5,260	7,810	6,250	1,820	7,920	1,540
V	206.0	233.0	209.0	1.2	255.0	93.7
Cr	44.8	240.0	228.0	38.8	38.3	804.0
Mn	795	1350	1160	338	601	670
Fe	60,300	66,500	61,000	29,600	44,800	36,200
Co	30.6	37.2	35.8	2.42	23.8	35.6
Ni	23.7	53.7	74.5	14.4	40.4	198.0
Cu	39.1	10.1	27.3	7.67	7.25	42.8
Zn	74.2	56.7	36.2	36.9	21.6	43.8
Ga	12.9	13.4	13.4	18.5	14.0	8.61
Rb	0.997	3.160	2.060	1.830	2.110	0.418
Sr	144	259	305	127	425	126
Y	21.5	28.2	25.2	46.1	20.3	5.4
Zr	78.1	73.6	67.2	66.4	46.4	13.2
Nb	2.15	2.47	2.12	6.05	2.96	1.08
Mo	0.376	0.593	0.386	1.040	0.575	0.647
Cd	0.205	0.0329	0.0192	0.0185	0.00772	0.0503
Sn	1.240	0.944	0.832	1.320	1.100	0.042
Sb	0.0582	0.0209	0.0232	0.0160	0.0126	0.0098
Cs	0.0279	0.0232	0.0050	0.0103	0.0482	0.0451
Ba	15.00	26.80	29.80	81.80	18.10	4.46
La	4.080	3.140	2.860	9.700	2.150	0.651
Ce	10.500	9.990	8.760	24.800	6.130	1.820
Pr	1.53	1.63	1.40	3.62	0.990	0.290
Nd	7.82	9.09	7.89	18.4	5.70	1.56
Sm	2.46	3.15	2.65	5.39	2.03	0.567
Eu	0.863	1.16	0.979	1.64	0.909	0.306
Gd	3.26	4.23	3.61	6.62	2.67	0.813
Tb	0.563	0.769	0.646	1.17	0.494	0.146
Dy	3.59	4.92	4.21	7.45	3.30	0.964
Ho	0.752	1.04	0.877	1.60	0.706	0.197
Er	2.15	2.92	2.55	4.62	2.03	0.571
Tm	0.335	0.448	0.409	0.724	0.338	0.090
Yb	1.94	2.75	2.52	4.46	2.07	0.546
Lu	0.272	0.380	0.358	0.643	0.297	0.079
Hf	2.10	2.05	1.90	2.31	1.46	0.394
Ta	0.131	0.145	0.120	0.289	0.163	0.031
W	0.103	0.0694	0.0575	0.113	0.473	0.044
Tl	0.0497	0.00299	0.00516	0.00750	0.00453	0.00167
Pb	0.730	0.227	0.135	1.17	0.284	0.236
Bi	0.0125	0.00443	0.00172	0.00261	0.00243	0.00462
Th	0.698	0.171	0.170	1.48	0.423	0.0425
U	0.486	0.0648	0.0719	0.579	0.216	0.0192

Concentrations are in parts per million by weight.